Nuclear Materials and Energy 12 (2017) 1336–1341

Contents lists available at ScienceDirect

Nuclear Materials and Energy

journal homepage: www.elsevier.com/locate/nme

Mechanical properties of tungsten following rhenium ion and helium plasma exposure

C.S. Corr[a,*], S. O'Ryan[a], C. Tanner[a], M. Thompson[a], J.E. Bradby[a], G. De Temmerman[b], R.G. Elliman[a], P. Kluth[a], D. Riley[c]

[a] Research School of Physics and Engineering, The Australian National University, Canberra 2601, Australia
[b] ITER Organization, Route de Vinon-sur-Verdon CS 90046- 13067 St Paul Lez Durance Cedex, France
[c] Australian Nuclear Science and Technology Organisation, Lucas Heights, NSW 2234, Australia

ARTICLE INFO

Article history:
Received 15 July 2016
Revised 19 March 2017
Accepted 22 April 2017
Available online 13 May 2017

ABSTRACT

Mechanical properties of Tungsten (W) samples irradiated with 2 MeV Rhenium (Re) ions and helium (He) plasma were investigated using nanoindentation. It was found that there was an increase in hardness for all samples following separate irradiation with both Re ion and He plasma. A slight increase in hardness was obtained for combined exposures. A comparable increase in hardness was observed for a pure He plasma with a sample temperature of 473 K and 1273 K. Optical interferometry was employed to compare surface modification of the samples. Grazing incidence small angle x-ray scattering confirmed He nano-bubble formation of approximately 1 nm diameter in the higher temperature sample, which was not observed with samples at the lower temperatures.

1. Introduction

Tungsten (W) has been chosen as the material for the ITER divertor and is a contender for the wall of DEMO, which will experience temperatures in excess of 1000 K. In such environments the material will be exposed to high flux helium (He) plasma as well as high energy neutrons. The interaction between high-flux He plasma with W can lead to plasma-induced surface morphology modifications. In particular He plasma interaction with W is known to form nano-scale bubbles beneath the surface, which could degrade the material performance [1–3]. The impact of both plasma and ion irradiation of the material surface can lead to changes in the mechanical properties, and is an important issue that is not well understood.

The effect of radiation damage of W using both high energy ions and high-flux plasma has been a subject of intense research in recent years. A particular focus has been on using nanoscale characterisation techniques such as nano-indentation to gain insight into changes in the mechanical properties of the material [4–7]. Armstrong et al. [4] investigated changes to the mechanical properties in pure W samples resulting from sequential self-ion implantation up to 13 dpa followed by He-ion implantation. A significant increase in hardness was observed in He implanted regions of the sample compared with smaller increases in hardness in the self-ion implanted regions. It was suggested that the self-ion implanted region contained pre-existing dislocation loops and that He trapped in distributed vacancies gives stronger hardening than He trapped in vacancies condensed into dislocation loops. Testing of He and self-implanted W yields an increase in the materials modulus of approximately 10% for self-implanted W, and 20% for combined He and self-implantation [6].

Recently Zhang et al. [8] used nano-indentation to investigate the hardening effect of as-received and recrystallised W samples using 6.4 MeV Fe^{3+} both with and without He^{+} at temperatures between 300 °C and 1000 °C. It was found that Fe^{3+} ion irradiation creates hardening in all W samples. Hardening due to the combined effect of Fe^{3+} and He^{+} was found to depend on the conditions of the W material. Recrystallised W was not affected by the addition of He^{+} irradiation while as-received W increased in hardness for all temperatures. In other work, Terentyev et al. [9] investigated surface hardening of W resulting from exposure to a high flux (10^{24} $D/m^2/s$.) Deuterium (D) plasma. The hardness-to-modulus ratio (H/E_r^2) was used as a measure of the resistance to plastic penetration and found to be greater following plasma exposure. Furthermore the reduced hardness $(H/H_0)^2$ was found to be higher in the plasma exposed

* Corresponding author.
E-mail address: cormac.corr@anu.edu.au (C.S. Corr).

http://dx.doi.org/10.1016/j.nme.2017.04.012

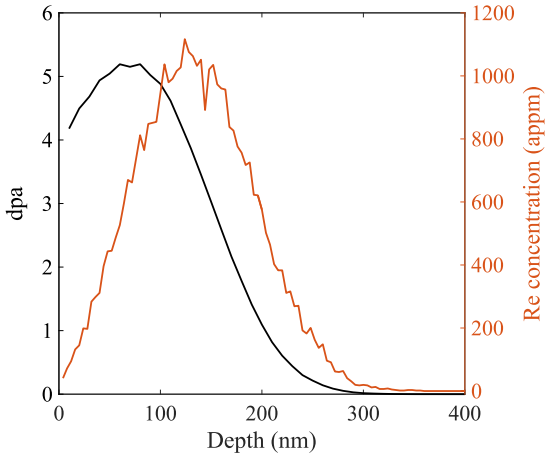

Fig. 1. Rhenium distribution and dpa as a function of depth calculated by the SRIM code for 2 MeV Rhenium ions.

samples within the probed depth. The increase in hardness was attributed to the presence of nanometric cavities, that were possibly filled with D, which provided extra resistance to the penetration of dislocations. Khan et al. [10] studied as-received and annealed W samples that were irradiated at a temperature of 400 °C with Re and W ions to create damage levels of 40 dpa. Using nano indentation, a 13% increase was observed in hardness was measured following irradiation of the as-received samples and a 23% increase for the annealed samples. There was negligible difference between the W and Re damaged samples. Electron Back Scatter Diffraction (EBSD) confirmed that the damage is dependent on the grain orientation [10].

In this work we investigate the effect that He plasma exposure and high-energy Re^{2+} ion beam irradiation have on W samples. The samples are analysed to determine the formation of defects and nano-bubbles and the influence that these have on the mechanical properties of W. The key material characterisation techniques employed are nano indentation to measure the mechanical properties of hardness and modulus, Grazing Incidence Small Angle X-Ray Scattering (GISAXS) to determine He nano-bubbles formation and optical interferometry to study surface modification.

2. Experimental setup and material characterisation

Plasma exposure was performed on the linear plasma device Magnum-PSI at the Dutch Institute For Fundamental Energy Research (DIFFER). The samples were maintained at floating potential and were exposed to surface temperature of 473 K and 1273 K. Samples were exposed to a He ion fluence of 2×10^{25} m^{-2} with ion energies less than 20 eV. This work investigated radiation damage of polycrystalline samples (10 mm x 10 mm x 2 mm) of 99.97% purity W (PLANSEE GmbH) with elongated grains orientated perpendicular to the sample surface. Surface preparation was performed using chemo-mechanical processing to ensure a low RMS roughness (0.1 µm), while maintaining a consistent surface topology. The effects of collision cascades and transmutation from neutron irradiation were simulated by irradiating the samples with 2 MeV Re^{2+} ions to a fluence of 10^{19} ions/m^2 at the 1.7 MV tandem ion accelerator at the Australian National University. All irradiations were performed at room temperature by rastering the beam across the sample surface. As shown in Fig. 1, these implantations created damage profiles with peak damage levels of approximately 5.2 displacements per atom (dpa) at a depth of 80 nm calculated using the Kinchin-Pease method with SRIM [11].

A Hysitron TriboIndenter was used to measure changes in the mechanical properties of each sample by determining the reduced Youngs modulus and the hardness of each sample. The nanoindenter has an operational load of up to 10 mN and a noise floor of less than 0.02 nm which allowed a highly precise measurement of the hardness and modulus of the material. For the measurements presented here a Berkovich tip was used. Many studies have been carried on the effect of surface roughness on nanoindentation, with the overall conclusion that surface roughness has two main effects [12,13]. The first is to increase the uncertainty in the measured results, by giving a larger variation across multiple indents in a sample. This will give a significantly larger spread in results than is desirable, but can be mitigated if a large enough sample size is taken. The second and most important effect of surface roughness on nanoindentation is the apparent increase in hardness and decrease in reduced Young's modulus. This effect can be reduced by penetrating to larger depths as the indenter will then be pushing through the rough surface and reach the bulk material. [14,15]. To account for the variation in hardness with surface roughening, nanoindentation was performed from depths of 190 nm to 240 nm on each sample by performing 49 indents. The indents were set up in a 7x7 square array with separation of 100 µm to allow for effects of grain boundaries and regional effects. The two arrays on each sample were separated to ensure they were independent and had no influence on the other measurements. A consistent loading function was applied to all of the indents. This consisted of a 10s increase from zero at initial contact through to 10 mN maximum force. This was followed by a hold of 10 s with a constant load of 10 mN, before the load was released at a constant rate of 10 s down to 0 N. This allowed the maximum penetration into the sample to ensure that the mechanical values given were due to effects below the initial surface layer and not just the surface. The hold function was used to allow for any material creep within the samples. The error in nanoindentation measurements were calculated from the standard deviation of several measurements at the same depth and was found to be less than 0.5%.

GISAXS was performed at the Australian Synchrotron using the SAXS/WAXS beamline. The measurements were taken with 10 keV x-rays and a camera length of 964 mm for different x-ray incident angles from 0° to 1°. GISAXS is a powerful non-destructive technique that can measure sub-surface nano-bubble size distributions. The diffraction model used in this work is described in detail in Thompson et al. [18]. A detailed description of the GISAXS technique and its application to measuring He nano-bubbles can be found in previous studies [16–19].

Optical Interferometry was used to provide a qualitative analysis of the surface with nm resolution. Along with these surface maps, values for the surface roughness were obtained which allowed a comparison between the different samples to be quantified. The surface characteristics of the samples were measured using a Wyko NT9100 Optical Profiler. This was setup using a 50X multiplication objective lens and an area of 500 µm × 500 µm was scanned for each sample. This was repeated for each sample twice on different sections of the sample to ensure regional effects were accounted for. After each sample was measured, results were exported in the form of a 3D surface map, a height distribution histogram, and a surface roughness value. The 3D surface map enables a qualitative understanding of effects on the surface while the height distribution histogram and surface roughness value enables a quantitative view of the surface.

3. Results

Fig. 2 shows variations in the surface topography measured by optical interferometry. The undamaged reference sample displays a smooth surface finish with very little variation across the sur-

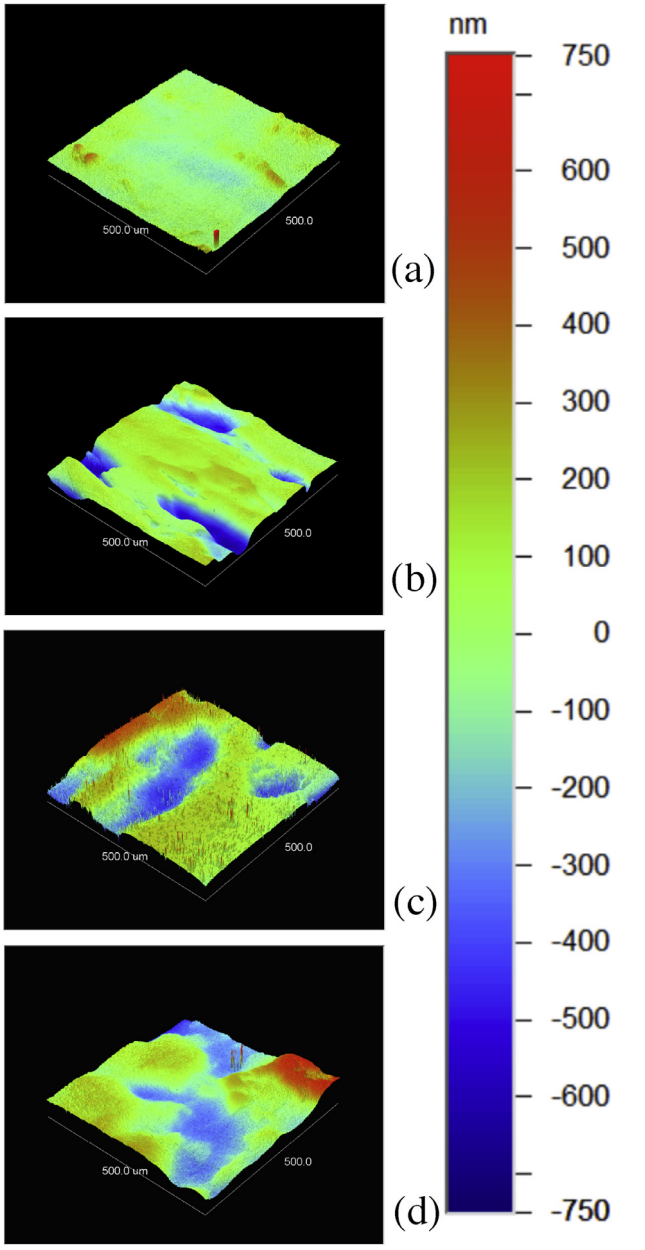

Fig. 2. Contour surface maps for (a) Reference sample, (b) Re^{2+} He (2 x 10^{25} ions/m^2 at 473 K), (c) He plasma only (2 x 10^{25} ions/m^2 at 473 K) and (d) He plasma only (2 x 10^{25} ions/m^2 at 1273 K). Surface Maps show a 500μm × 500μm section of the sample with the vertical scale from 750 nm to 750 nm.

face (Fig. 2a). Implanting with Re ions only in the sample resulted in little change to the surface. Fig. 2b shows that Re ion irradiation followed by He plasma exposure at low temperature results in trenches being created across the W surface. As shown in Figs. 2c and 2d, a major modification of the surface results for He plasma with low (473 K) and high (1273 K) surface temperatures. There is a suggestion of significant nano-scale modification for the sample at 473 K which is confirmed by SEM images (Fig. 3a). At such low sample temperature, nano fuzz is not expected to occur. The high resolution SEM in Fig. 3b shows structures that are similar to the "nano-tendril bundles" observed by Woller et al. [20]. Woller et al. observed that at temperatures lower than that necessary for fuzz formation (870 to 1220 K), nano-tendril bundles can form on the surface and is dependent on the average ion energy and ion

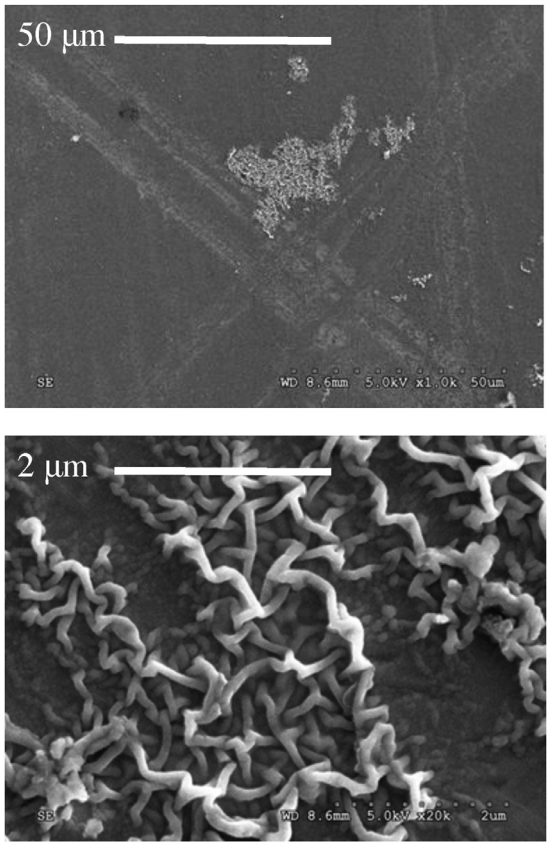

Fig. 3. SEM image of surface morphology changes due to plasma exposure for He plasma only at a fluence of 2 x 10^{25} ions/m^2 at 473 K for two magnifications.

flux density. This nano-structuring of the surface requires further investigation.

Fig. 4 displays SEM images of samples exposed to (a) a pure hydrogen (H) plasma, (b) mixed 50:50 H/He plasma, and (c) a pure He plasma for a surface temperature of 1273 K and fluence of 2 x 10^{25} ions/m^2. It is observed that the greatest nano-structuring of the surface occurs for the pure He plasma exposure. As shown by Khan et al. [21] W fuzz may be created at higher surface temperatures, however, fuzz was not observed during this investigation.

Nanoindentation is a method of studying the mechanical properties of a material by pressing a small tip into the material. Similar to the methods used for calculating hardness using a Vickers or Brinell test, nanoindentation produces measurements on a nanometre scale rather than the conventional micron or millimetre scale. By knowing the dimensions of the tip, the depth of penetration can be used to calculate mechanical properties of the material such as hardness, modulus, strain-hardening exponent, and fracture toughness [22]. Since the residual indent produced is on the nanometre scale, nanoindentation is considered a non-destructive testing method as the changes made to the material through the testing method will not alter its overall properties. The hardness and reduced Young's modulus are calculated during a cycle of loading and unloading of the tip into the material [23]. From this curve we can obtain the contact stiffness S, and the maximum load P_{max}. The hardness of the material is then defined by the equation:

$$H = \frac{P_{max}}{A} \tag{1}$$

where A is the projected area (which is calculated as the geometry of the tip is known). The reduced Young's modulus is calculated

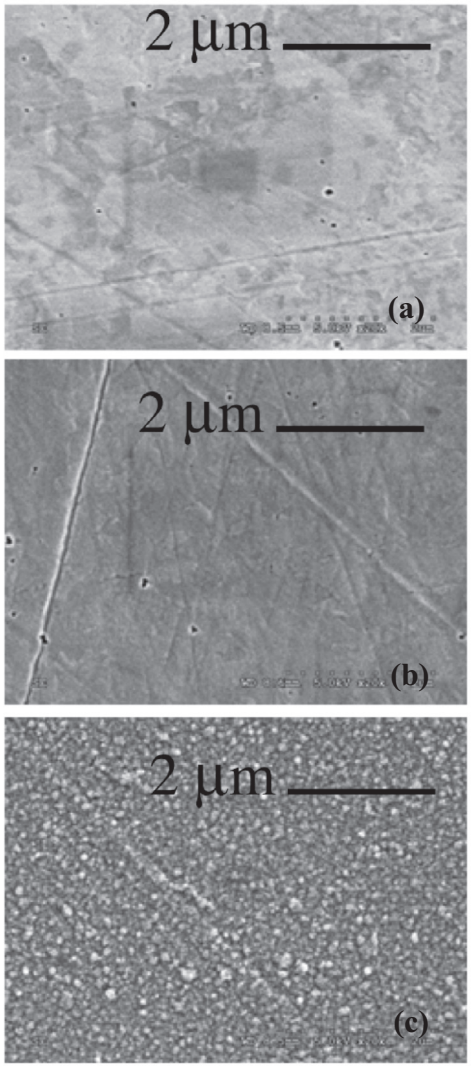

Fig. 4. An example of SEM images of surface morphology changes due to plasma exposure for (a) pure H plasma, (b) mixed H/He plasma (50%), and (c) pure He plasma at 1273 K and fluency of 2 x 10^{25} ions/m^2.

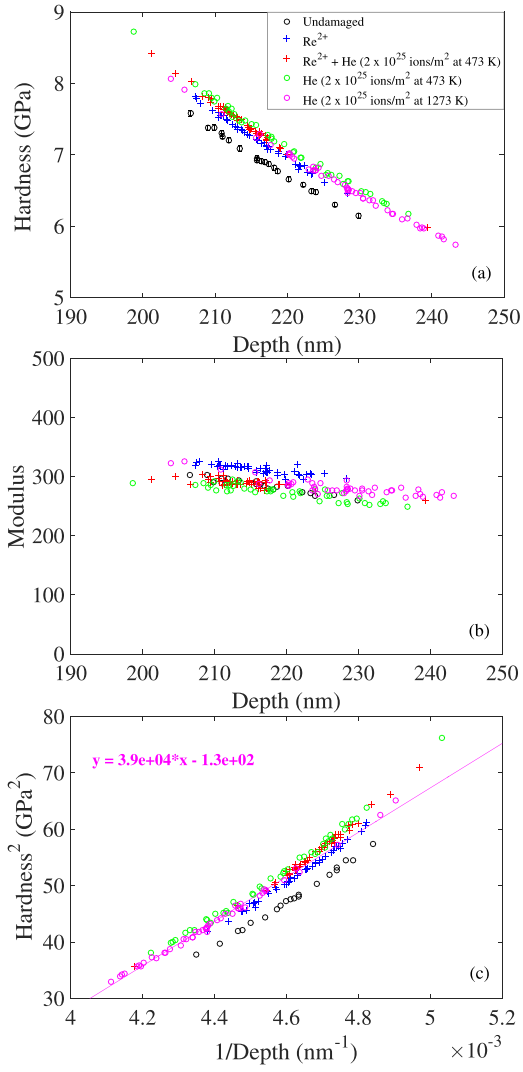

Fig. 5. (a) Profile measurements of the hardness as a function of depth. (b) Profile measurements of the modulus as a function of depth. (c) A plot of hardness^2 versus the reciprocal of the depth. The line demonstrates the Nix–Gao relationship for the case of He plasma exposure (2 x 10^{25} ions/m^2 at 1273 K).

through the equation

$$E_r = \frac{\sqrt{\pi}}{2\beta}\frac{S}{\sqrt{A}} \tag{2}$$

where β is constant determined by the shape of the indenter tip. The reduced Young's modulus is reduced as it takes into account the elastic changes in the tip and the material. This is defined by the relationship below where ν is the Poisson's ratio of the material

$$\frac{1}{E_r} = \frac{1-\nu^2_{material}}{E_{material}} + \frac{1-\nu^2_{tip}}{E_{tip}} \tag{3}$$

The mechanical properties of the samples before and after irradiation are summarised in Fig. 5. The properties were investigated for depths between 190 nm and 240 nm to avoid uncertainties due to surface roughness. At these depths the damage level is approximately 1 dpa. Although the hardness for the various samples are close, there are some minor differences and trends that are discussed here. Fig. 1a displays the variation of hardness as a function of depth. A comparable increase is observed for all sample irradiation. There is a 3% increase in hardness following irradiation of the sample using the Re ions only. With the addition of the He plasma exposure there is a further increase in hardness up to 5%. The observed increase is much greater than the standard deviation of 0.5%. This increase in hardness created under Re ion irradiation may be the result of dislocation loops [10]. Plasma exposure may then result in He-filled vacancies further increasing the hardness. It is interesting to note that pure He exposure resulted in similar values of hardness. Fig. 5b displays the modulus as a function of depth for all samples. The modulus remains fairly unchanged for all samples studied here. Furthermore the modulus remains constant with indentation depth, in contrast to the hardness profile.

The decrease in hardness with increasing indent depth is often explained by the Nix Gao model, which accounts for higher hardness being observed at shallow depths compared with deeper depths. A system follows the Nix and Gao model states if the square of the hardness is directly proportional to the reciprocal of the indentation depth. This relationship is illustrated in Fig. 5c. The line demonstrates the Nix-Gao relationship for the case of He plasma exposure only (2 x 10^{25} ions/m^2 at 1273 K). It can be seen that the trends closely follow the relationship.

In this work GISAXS was used to investigate the formation of He nano-bubbles. Fig. 6 displays a summary of the GISAXS patterns obtained for different samples. The scattering pattern for the

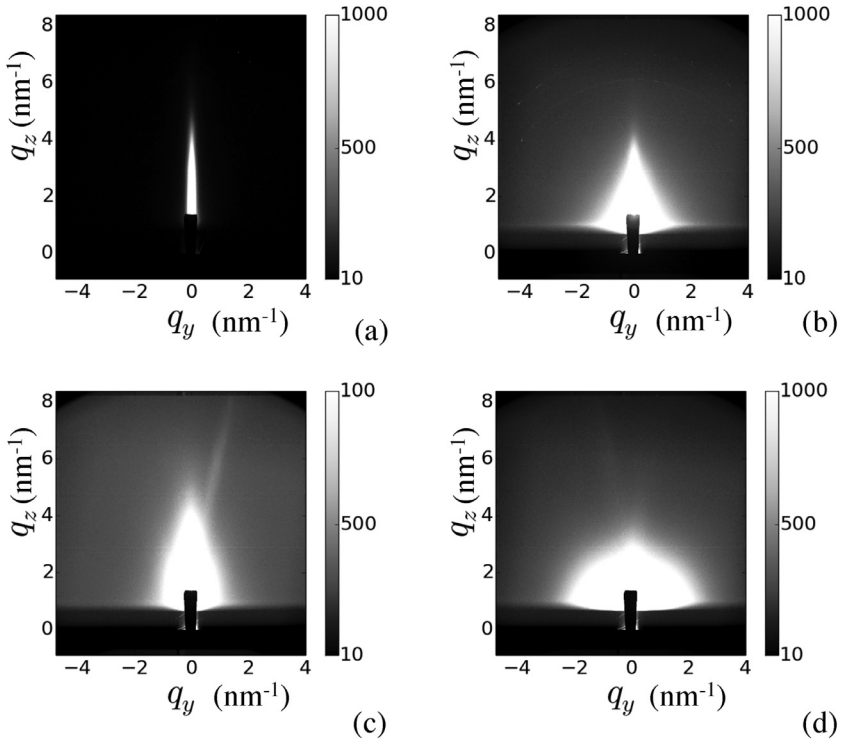

Fig. 6. GISAXS patterns for (a) Reference sample, (b) Re^{2+} + He (2 x 10^{25} ions/m^2 at 473 K), (c) He plasma only (2 x 10^{25} ions/m^2 at 473 K) and (d) He plasma only (2 x 10^{25} ions/m^2 at 1273 K). The circular contribution in (d) demonstrates nano-bubble formation.

undamaged sample shows a bright streak aligned along the central axis. Irradiation of the W sample with Re ions + He plasma results in a broadening of this streak possibly due to surface modification. This is also similar for the He plasma exposure at low surface temperatures. In comparison, the higher temperature sample exposed to He plasma displays a diffuse circular pattern indicating the formation of He nano-bubbles on the order of a few nanometres in diameter [16–18]. Nano-bubbles were not observed in other samples, likely as a result of the very low levels of He retention. This is believed to be a consequence of the low ion temperatures for these plasmas, which reduced the implantation energy of the ions below the threshold required for He retention [19].

4. Conclusion

In this work, we investigated the effect that Re ion and plasma irradiation has on W samples. It was found that the hardness increases for all samples relative to the unmodified reference while there was little variation in the modulus. While no nano bubbles were measured for low sample temperatures with He plasma exposure, nano bubbles of approximately 1 nm diameter were detected in the higher temperature sample. The results suggest that He trapped in vacancies and the formation of He nano bubbles in the W matrix results in increased material hardness. Future work will include measuring using Positron Annihilation Lifetime Spectroscopy to detect voids and early stages of bubble formation.

Acknowledgments

GISAXS work was undertaken on the SAXS/WAXS beam line at the Australian Synchrotron, Victoria, Australia. Heavy-ion irradiation was performed at the ANU node of the Heavy-Ion-Accelerator Capability funded by the Australian Government under the NCRIS program. The DIFFER authors were supported by the research programme of the Stichting voor Fundamenteel Onderzoek der Materie (FOM), which is financially supported by the Nederlandse Organisatie voor Wetenschappelijk Onderzoek (NWO). PK, CC and JB acknowledge support from the Future Fellowship Scheme of the Australian Research Council (FT120100289, FT100100825 and FT130101355). This research has also been supported by the Science and Industry Endowment Fund grant (PS034). The views and opinions expressed herein do not necessarily reflect those of the ITER Organisation.

References

[1] M. Miyamoto, S. Mikami, H. Nagashima, N. Iijima, D. Nishijima, R.P. Doerner, N. Yoshida, H. Watanabe, Y. Ueda, A. Sagara, J. Nucl. Mater. 463 (2015) 333–336.
[2] S. Kajita, N. Yoshida, R. Yoshihara, N. Ohno, M. Yamagiwa, J. Nucl. Mater. 418 (2011) 152–158.
[3] D. Nishijima, M.Y. Ye, N. Ohno, S. Takamura, Formation mechanisms of bubbles and holes on tungsten surface with low-energy and high-flux Helium plasma irradiation in NAGDIS-II, J. Nucl. Mater. 329–333 (2004) 1029–1033.
[4] D.E.J. Armstrong, P.D. Edmondson, S.G. Roberts, Effects of sequential tungsten and Helium ion implantation on nano-indentation hardness of tungsten, Appl. Phys. Lett. 102 (2013) 251901.
[5] D.E.J. Armstrong, A.J. Wilkinson, S.G. Roberts, Mechanical properties of ion-implanted tungsten5wt% tantalum, Physica Scripta T145 (2014) 1–3.
[6] J. Gibson, D. Armstrong, S. Roberts, Òthe micro-mechanical properties of ion irradiated tungsten, Physica Scripta 159 (2011) 1–5.
[7] D.E.J. Armstrong, C.D. Hardie, J.S. Gibson, A.J. Bushby, P.D. Edmondson, S.G. Roberts, Small-scale characterisation of irradiated nuclear materials: part II nanoindentation and micro-cantilever testing of ion irradiated nuclear materials, J. Nucl. Mater. 462 (2015) 374–381.
[8] Z. Zhang, E. Hasenhuetl, K. Yabuuchi, A. Kimura, Evaluation of Helium effect on ion-irradiation hardening in pure tungsten by nano-indentation method, Nucl. Mater. Energy 000 (2016) -8.
[9] D. Terentyev, A. Bakaeva, T. Pardoen, A. Favache, E.E. Zhurkin, Surface hardening induced by high flux plasma in tungsten revealed by nano-indentation, J. Nucl. Mater. 476 (2016) 1–4.
[10] A. Khan, R. Elliman, C. Corr, J.J.H. Lim, A. Forrest, P. Mummery, L.M. Evans, Effect of Rhenium irradiations on the mechanical properties of tungsten for nuclear fusion applications, J. Nucl. Mater. 477 (2016) 42–49.
[11] J.F. Ziegler, M.D. Ziegler, J.P. Biersack, SRIM the stopping and range of ions in matter (2010), Nucl. Instruments Methods Phys. Res. Sect. B Beam Interact. with Mater. Atoms 268 (2010) 181823.
[12] J.Y. Kim, S.K. Kang, J.J. Lee, J. Jang, Y.H. Lee, D. Kwon, Influence of surface-roughness on indentation size effect, Acta Materialia 55 (2007) 3555–3562.

[13] L. Chen, A. Ahadi, J. Zhou, J.E. Stahl, Modeling effect of surface roughness on nanoindentation tests, Procedia CIRP 8 (2013) 334–339.
[14] A.C. Fischer-Cripps, Nanoindentation, Springer, Lindfield, 2000.
[15] T.Y. Zhang, W.H. Xu, M.H. Zhao, The role of plastic deformation of rough surfaces in the size-dependent hardness, Acta Materialia 52 (2004) 57–68.
[16] M. Thompson, R. Sakamoto, E. Bernard, N. Kirby, P. Kluth, D. Riley, C. Corr, GISAXS modelling of Helium-induced nano-bubble formation in tungsten and comparison with TEM, J. Nucl. Mater. 473 (2016) 612.
[17] M. Thompson, P. Kluth, R.P. Doerner, N. Kirby, C. Corr, Probing Helium nano-bubble formation in tungsten with grazing incidence small angle x-ray scattering, Nucl. Fusion 55 (2015) 42001.
[18] M. Thompson, P. Kluth, R.P. Doerner, N. Kirby, D. Riley, C.S. Corr, Measuring Helium bubble diameter distributions in tungsten with grazing incidence small angle x-ray scattering (GISAXS), Phys. Scr. T167 (2016a) 014014.
[19] M. Thompson, A. Deslandes, T.W. Morgan, R.G. Elliman, G. De Temmerman, P. Kluth, D. Riley, C.S. Corr, Observation of a Helium ion energy threshold for retention in tungsten exposed to hydrogen/Helium mixture plasma, Nucl. Fusion 56 (2016b) 104002.
[20] K.B. Woller, D.G. Whyte, G.M. Wright, Impact of Helium ion energy modulation on tungsten surface morphology and nano-tendril growth, in: 26th IAEA Fusion Energy Conference, MPT/P5-26, 2016.
[21] A. Khan, G. De Temmerman, T.W. Morgan, M.B. Ward, Effect of Rhenium addition on tungsten fuzz formation in Helium plasmas, J. Nucl. Mater. 474 (2016) 99–104.
[22] A.C. Fischer-Cripps, Nanoindentation, Springer, Lindfield, 2000.
[23] W.C. Oliver, G.M. Pharr, Measurement of hardness and elastic modulus by instrumented indentation: advances in understanding and refinements to methodology, J. Mater. Res. 19 (2004) 3–20.